Electronic Supplementary Material (ESI) for Chemical Science

Assembly of Mesoporous Indium Tin Oxide Electrodes from Nano-Hydroxide Building Blocks

Yujing Liu, Goran Štefanić, Jiří Rathouský, Oliver Hayden, Thomas Bein, Dina Fattakhova-Rohlfing

Supplementary information

Table S1
Output of the PRO-FIT program giving the refined least-squares parameters (the Bragg angle positions ($2\theta_B$)), FWHM values and integrated intensities of the diffraction lines) for the as-prepared indium tin hydroxide in the three selected 2θ regions containing 5 to 6 diffraction maxima.

Line	Individual profile fitting results (PRO-FIT)			
	$2\theta_B$	FWHM	Integrated intensity	R_{wp}
1	18.69(2)	2.86(7)	37549±1067	0.022
2	22.34(1)	1.17(1)	80634±744	
3	24.85(1)	2.87(3)	136284±1436	
4	28.97(1)	2.66(5)	43302±910	
5	33.66(1)	2.45(3)	71576±946	
6	36.41(3)	2.68(3)	19849±503	
7	41.12(2)	2.37(4)	10235±231	0.020
8	45.51(1)	1.21(2)	11001±239	
9	49.24(1)	3.45(2)	64069±338	
10	52.60(1)	3.06(2)	65540±399	
11	54.75(1)	3.86(2)	87257±414	
12	58.16(3)	2.67(7)	12931±313	
13	63.67(4)	1.72(9)	1546±102	0.015
14	69.60(1)	3.69(2)	30827±178	
15	73.42(3)	3.51(5)	10196±142	
16	76.76(1)	3.20(2)	26328±163	
17	80.64(2)	2.32(5)	4651±147	

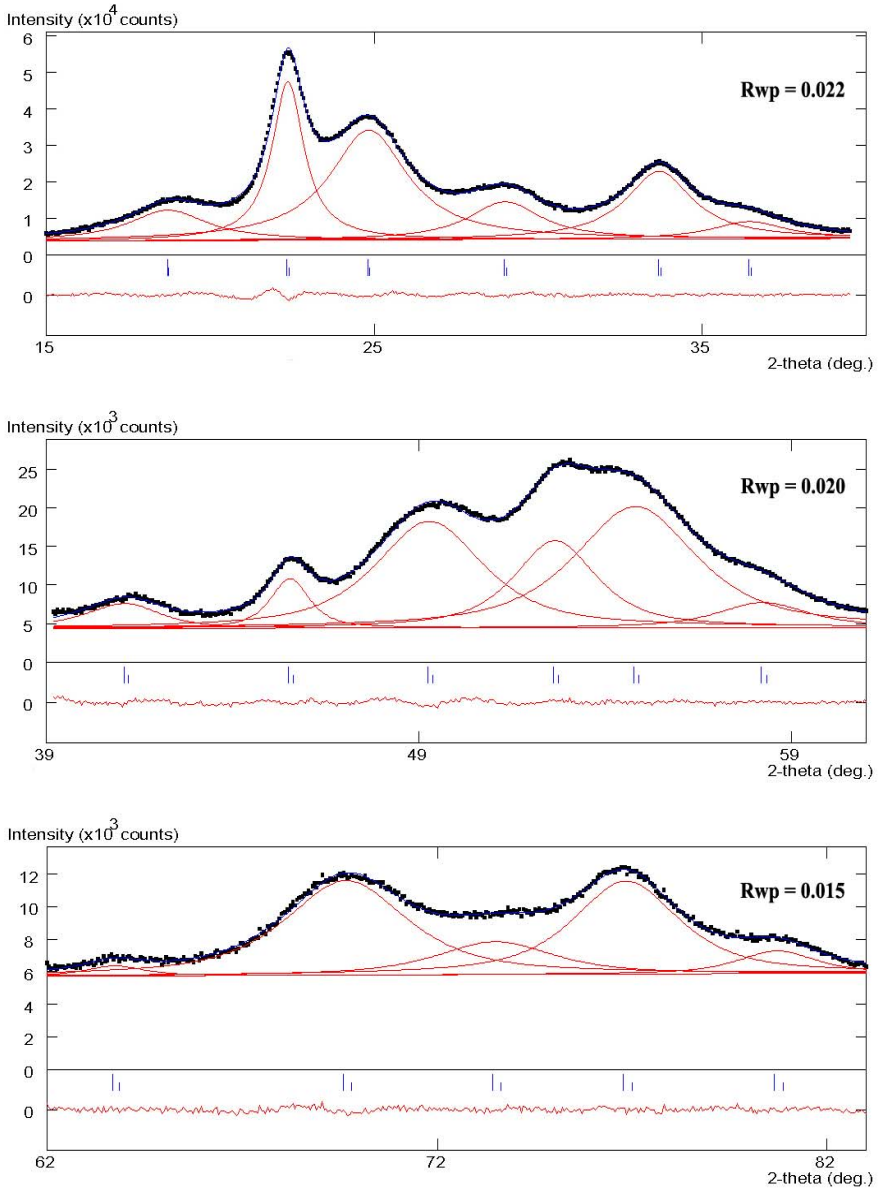

Figure S1. Individual profile-fitting results for the as-prepared indium tin hydroxide in the three selected 2θ regions containing 5 to 6 diffraction maxima. The observed data are represented by black squares, the calculated profile for each diffraction line by red lines, the total calculated profile by a blue line, the difference between the observed and calculated profile by the red line at the bottom of the diagram on the same scale as the above. Long and short vertical bars mark the Cu $K\alpha_1$ and Cu $K\alpha_2$ positions of the reflections, respectively.

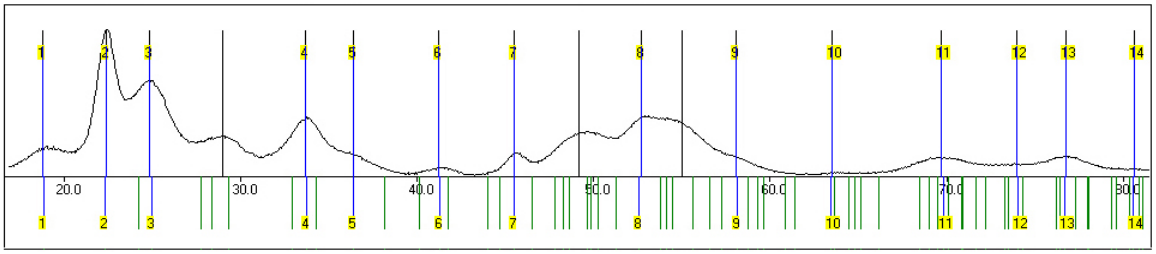

Figure S2. Relation between positions of the diffraction maxima in the XRD pattern of the as-prepared indium tin hydroxide and calculated diffraction line positions for the hexagonal lattice proposed by Qiu *et al.*[1] (program CheckCell). Black vertical bars above and green vertical bars below mark the positions of the observed and calculated diffraction lines, respectively. In case where the positions of the observed and calculated lines are almost the same (within a 2θ range of ±0.15°) the color of the bars is blue.

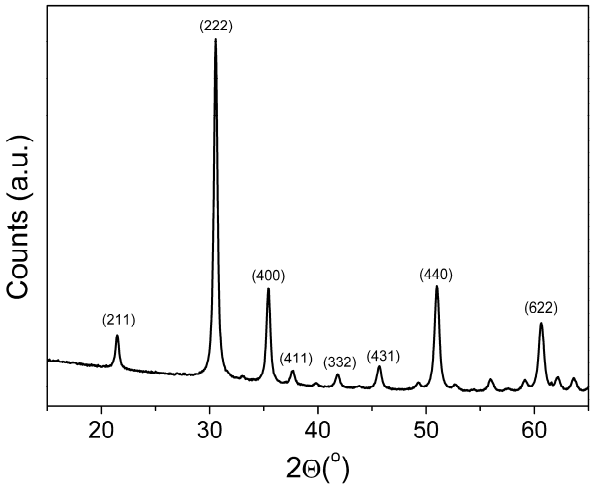

Figure S3. XRD pattern of indium tin hydroxide nanoparticles after calcination at 400 °C in air.

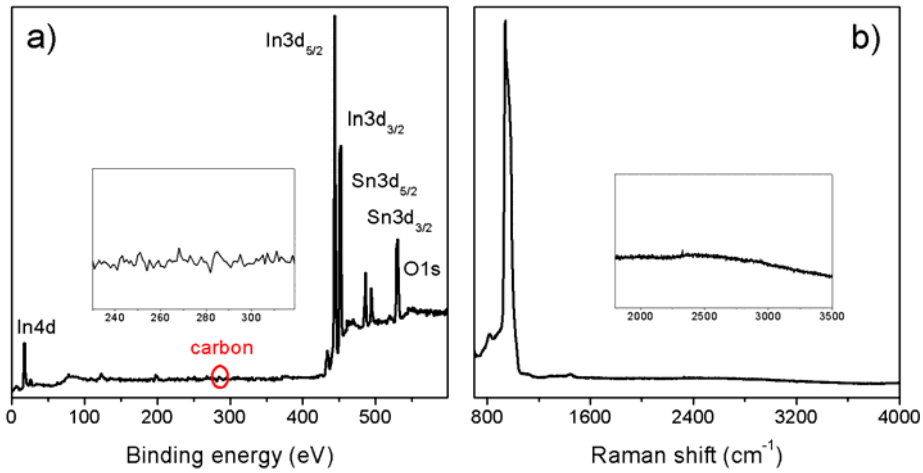

Figure S4. XPS (a) and Raman (b) spectra of the ITO films assembled from nano-hydroxides after calcination at 300 °C in air and heating at 300 °C in forming gas. The inset in (a) zooms in the energy region corresponding to carbon, indicating that no carbon residuals are present on the surface, and the inset in (b) zooms in the region between 1800 and 3500 cm^{-1} showing the absence of stretching vibrations of the aliphatic groups characteristic for Pluronic polymer.

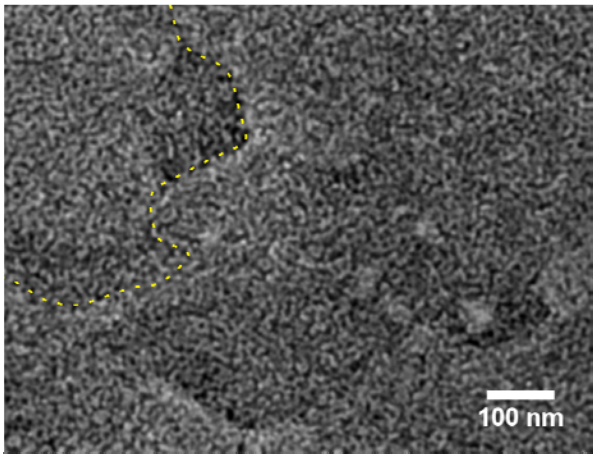

Figure S5. Top view SEM image of monolayer mesoporous ITO film assembled from indium tin hydroxide nanoparticles after calcination at 300 °C in air and heating at 300 °C in forming gas. The yellow dashed line outlines an edge of terrace-like crystalline domains of the underlaying dense ITO film taken as a substrate.

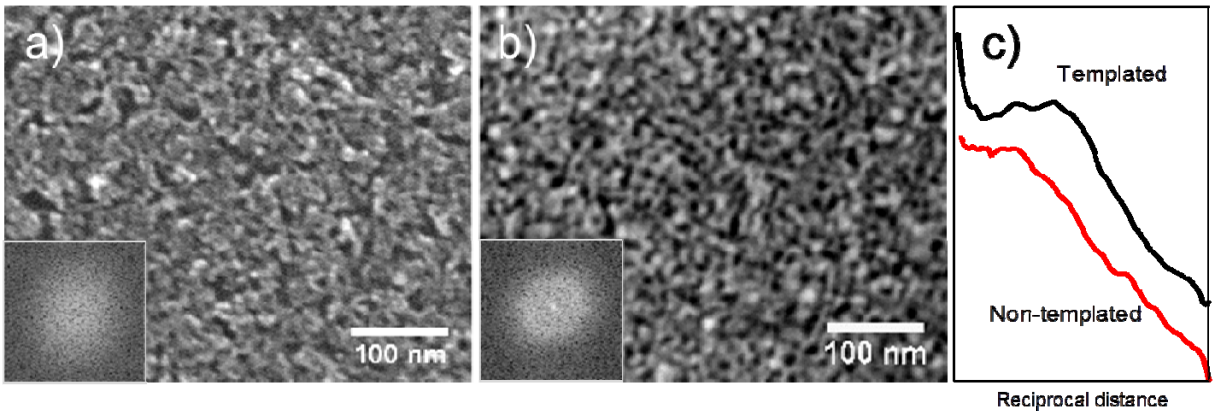

Figure S6. Top view SEM image of ITO film assembled from indium tin hydroxide nanoparticles without (a) and with (b) addition of Pluronic F127 in the coating solution. Both films were calcined at 300 °C in air and heated at 300 °C in forming gas. The insets show the Fourier transforms of the images with the corresponding intensity profiles shown in (c).

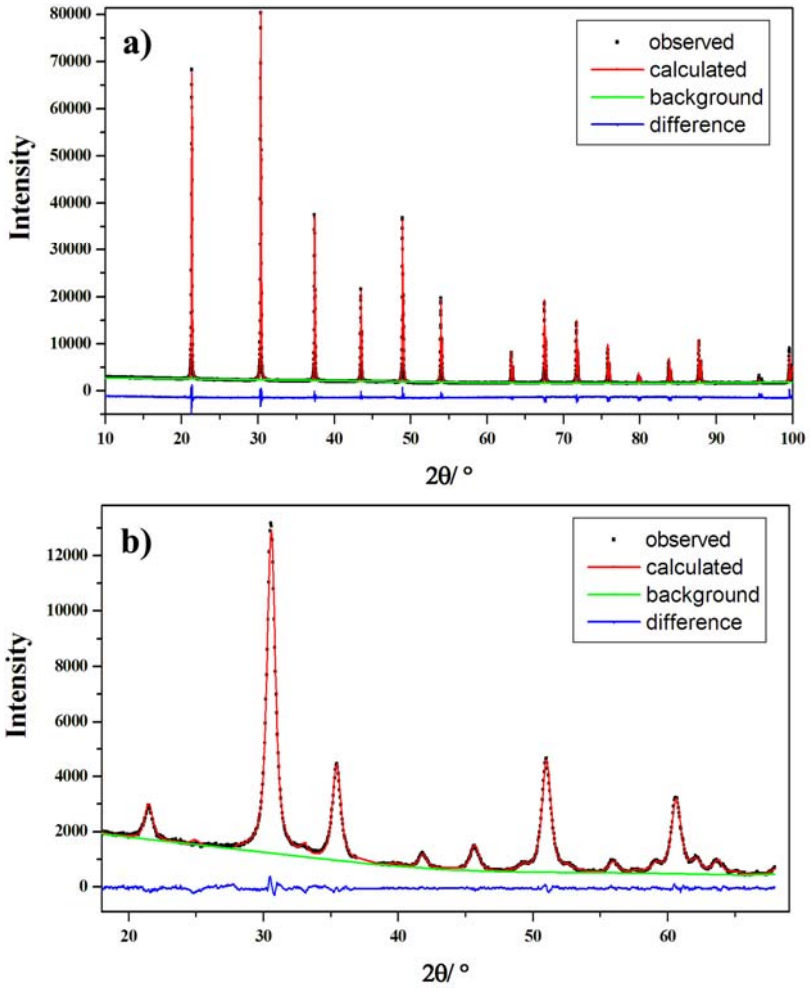

Figure S7. Result of the whole-powder-pattern profile refinement of (a) LaB_6 standard (R_{wp} = 0.050), used for the determination of the instrumental profile in line-broadening analysis, and (b) the mesoporous ITO film prepared from the preformed nano-hydroxides and treated at 300 °C in air followed by a treatment at 300 °C in N_2/H_2 (R_{wp} = 0.025). In the refinement of the ITO sample 2θ regions from 37.0° to 38.5° and from 43.2° to 44.5° were excluded due to the presence of diffraction lines of the substrate.

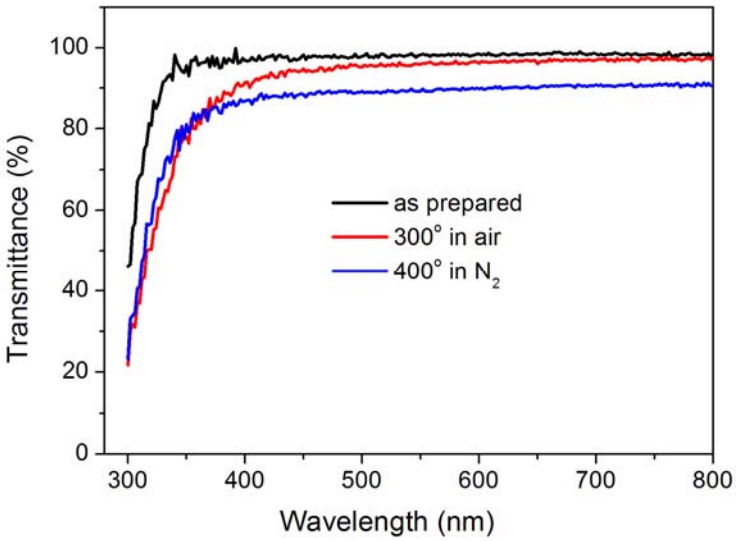

Figure S8. UV/vis absorption spectra of the ITO films assembled from nano-hydroxides: as prepared (black line), heated at 300 °C in air (red line) and additionally for 400 °C in N_2 (blue line). The films were deposited on a borosilicate glass substrate; film thickness 300 nm.

Experimental part

Synthesis of nanoparticles and mesoporous films

Nanoparticles of indium tin hydroxide were prepared by a solvothermal synthesis using indium(III) chloride and tin(IV) chloride as metal oxide precursors, ethylene glycol (EG) as a solvent, and sodium hydroxide as a hydrolysis reagent. In a typical procedure, 0.091 g (0.35 mmol, 0.04 mL) of tin (IV) chloride (Aldrich) was added to a clear solution of 0.698 g (3.15 mmol) of indium (III) chloride (ABCR) in 7 mL (0.13 mmol) of ethylene glycol (Sigma-Aldrich, ≥99%, used without further drying). The molar ratio of tin and indium was 1:9 (mol:mol). Separately, 0.420 g (10.5 mmol) of sodium hydroxide (Aldrich, 97%) was dissolved in 7 mL (0.13 mmol) of EG at 0 °C. Both solutions were mixed at 0 °C and stirred for another 15 minutes. The mixture was transferred into a Teflon-lined autoclave and kept in a laboratory oven for 28 hours at 200 °C. The formed product was separated by centrifugation (50000 rcf, 20 min) and washed twice with bi-distilled water (Milli-Q Academic A10), being separated by centrifugation after each washing step. The washing steps have to be performed quickly in order to prevent re-dispersion of the nanoparticles. The solid part resulting from centrifugation was collected and used without drying for the preparation of colloidal solutions. The solid content of the collected material could differ for different synthesis batches; it was determined for each new batch either by weighing of a certain amount before and after evaporation of water, or using thermogravimetric analysis. The average solid content in the washed nanoparticles after centrifugation was 50 ± 10 %.

For the fabrication of mesoporous films, the wet nanoparticles containing 90 mg of solid indium tin hydroxide were first re-dispersed in 0.5 ml (27 µmol) of water to result in a slightly turbid colloidal dispersion, which turned transparent after the addition of 0.2–0.5 ml of concentrated acetic acid depending on the concentration of nanoparticles in the colloidal solution. Afterwards, 30 mg (2.6 µmol) of Pluronic F127 (Sigma) was dissolved in the particle dispersion. The resulting clear solutions were deposited on different substrates such as glass, ITO-coated glass or Si wafers (1.5 cm x 2 cm) by dip-coating (withdrawal speed 6 mm/s) or spin-coating (30 - 50 µL per 1 cm² substrate area) at 1000 rpm for 30 seconds. The dried films were heated to 300 °C in air (with a ramp of 0.5 °C/min) for 2 hours. For improvement of electrical conductivity, template-free mesoporous ITO films were further annealed in

inert N_2 or reducing forming gas (5% H_2/N_2) atmosphere at 300 to 500 °C (with a ramp of 1 °C/min) for 30 min.

For electrochemical characterization, the mesoporous ITO films were deposited on a conducting ITO-coated glass substrate by spin-coating as described above. Functionalization of ITO films was performed in two ways. For electrostatic anchoring of potassium hexacyanoferrate $K_3[Fe(CN)_6]$, the films were immersed first in a 0.20 wt% solution of poly(diallyldimethylammoniumchloride) (PDDA, MW 100.000 - 200.000) in water for 12 hours at room temperature. The PDDA-modified mesoporous ITO films were then stirred in a 10 mM $K_3[Fe(CN)_6]$ aqueous solution for 6 hours. The electrode was washed twice with bi-distilled water after each functionalization step. For electrochemical measurements, 0.1 M KCl in water was used as electrolyte. For the covalent anchoring of ferrocene moieties, the mesoporous ITO films were treated first in a 20 mM solution of 3-aminopropyltriethoxysilane (APTES) in dichloromethane under reflux for 3 h, followed by washing twice with dichloromethane. The APTES-functionalized films were stirred under reflux for 3 h in a 0.2 mM solution of ferrocene carboxylic acid and a 2 mM solution of N,N-dicyclohexylcarbodiimide in dichloromethane under reflux for 3 h and washed twice with dichloromethane. For electrochemical measurements, 0.5 M $LiClO_4$ in acetonitrile was used as electrolyte.

Characterization of nanoparticles and mesoporous films

Transmission electron microscopy (TEM) was performed using a FEI Titan 80-300 instrument equipped with a field emission gun. Due to the fast decomposition of hydroxide nanoparticles in the electron beam, the measurements were performed at 80 kV. The particulate samples were prepared by evaporating a drop of a diluted suspension of particles in water on a Plano holey carbon-coated copper grid. TEM of films was carried out by removing the thin-film samples from the substrate and transferring them onto a holey carbon-coated copper grid. Scanning electron microscopy (SEM) was performed on a JEOL JSM-6500F scanning electron microscope equipped with a field emission gun operated at 4 kV.

X-ray diffraction measurements at small and wide angle were carried out in reflection mode using a Bruker D8 Discover diffractometer with Ni-filtered CuK_α-radiation (λ = 1.5406 Å), and equipped with a Vantec-1 position-sensitive detector. XRD patterns of the unknown tin-doped indium hydroxide phase were analyzed with computer programs PRO-FIT[2] and CheckCell (a software performing automatic cell/space group determination).[3] The Bragg angle position ($2\theta_B$), integrated intensities and FWHM values of the diffraction lines (Table S1) were determined by using the individual profile fitting method with program PRO-FIT and taken as input data for the program CheckCell. The pseudo-Voigt profile function defined by Wertheim et al.[4] and a second order polynomial model for background intensity were used in the refinement. Due to the significant overlap of broad diffraction lines, the values extracted by program PRO-FIT (Table S1) were obtained after individual refinement of 2θ regions (~ 20°) containing 5 to 6 diffraction lines.

The particle size d of indium tin hydroxide nanoparticles was estimated from the broadening of the diffraction lines with $2\theta_B$ positions at 22.3° and 45.5° in the XRD pattern using the Scherrer equation $d = K\lambda/(B\cos\theta_B)$, where B is the full width at half maximum (FWHM) of a diffraction line corrected for the corresponding FWHM value for a standard, θ_B is the diffraction angle and K is the Scherrer's constant (about 0.9), and from the HRTEM images. The particle size in HRTEM was measured by visual inspection of ca. 100 particles.

A more accurate crystalline domain size determination from a line-broadening analysis of XRD patterns was performed by using two different methods: whole-powder-pattern profile refinements (Le Bail method,[5] program GSAS[6] with graphical user interface EXPGUI[7]) and double-Voigt method[8] (programs SHADOW[9] and BREDTH[10]). The results of whole-powder-pattern profile refinements were obtained by

following the procedure proposed in the Size/Strain Round Robin.[11] In the refinement we used a modified pseudo-Voigt function defined by Thompson et al,[12] which gave the following expression for Gaussian and Lorentzian observed line widths:

$$\Gamma_G^2 = U\tan^2\theta + V\tan\theta + W + P/\cos^2\theta \qquad (1)$$

$$\Gamma_L = (X + Xe\cos\phi)/\cos\theta + (Y + Ye\cos\phi)\tan\theta + Z \qquad (2)$$

where Γ is the full width at half maximum (FWHM) of the line profile, *U, V, W, P, X, Y, Z, Xe* and *Ye* are refinable parameters. The size and strain contribution to the line broadening can be given by the following equation:

$$\beta_S = \lambda/(D_V\cos\theta) \qquad (3)$$

$$\beta_D = e\,4\tan\theta \qquad (4)$$

where λ is the wavelength, D_v is the volume-averaged domain size, e represents the upper limits of micro-strain, while β_S and β_D represent the integral breadths of the Voigt function resulting from size and strain contribution, respectively. By comparing the equations (1) and (2) with the equations (3) and (4) it is easy to recognize that parameters *X, Xe* and *P* will relate to size broadening and *Y, Ye* and *U* to strain broadening. Therefore only those 6 profile parameters were refined in the Le Bail refinements of ITO samples, while all other profile parameters assumed the values obtained upon the refinement of the LaB_6 standard (Fig. S7). In order to obtain pure physically broadened profile parameters, used in the calculation of β_S and β_D values, the obtained values of the refined parameters *U, X, Y, P* for the samples were corrected by the corresponding values obtained for the standard.[11] (See Ref. 11 for a more detailed description of the whole procedure).

In the double-Voigt method,[8] which is equivalent to the Warren-Averbach approach,[13] both area- and volume-weighted domain size and the root-mean-square strain (RMSS) were calculated from 'pure' physically (specimen, structurally) broadened diffraction-line profiles of several most prominent diffraction lines (program BREADTH[10]). Pure physically broadened diffraction-line profiles were obtained by varying the parameters of the Voigtian profile shape function convoluted with the instrumental profile (split Person VII function fitted to the diffraction lines of LaB_6 standard) to obtain the best fit to the observed data[14] (program SHADOW).[9]

Textural properties of the mesostructured films were analysized by Kr sorption measurements at 77 K using an ASAP 2010 apparatus (Micromeritics). Porosity of the films was determined from the measured pore volume related to the volume of the film (calculated from exposed film area and the film thickness). The pore size distribution was calculated according to a procedure describe elsewhere.[15] Film thickness was determined using a profilometer Veeco Dektak 150 equipped with a diamond stylus (12.5 µm radius) in contact mode. The TGA analysis was performed on a Netzsch STA 440 C TG/DSC (heating rate of 1 K/min in a stream of synthetic air of 25 ml/ min).

The dispersion behavior of nanoparticles was studied by dynamic light scattering using a Malvern Zetasizer-Nano equipped with a 4 mW He-Ne laser (633 nm) and an avalanche photodiode detector.

XPS (X-ray photoelectron spectroscopy) analysis of the template-free mesoporous ITO films on silicon substrates was performed using a VSW HA 100 electron analyzer and the Kα radiation provided by a non-monochromatized aluminum anode system (Al Kα = 1486.6 eV). Raman spectra were recorded with a LabRAM HR UV-VIS (Horiba Jobin Yvon) Raman microscope (Olympus BX41) with a Symphony CCD detection system using a HeNe laser at 632.8 nm.

DC electrical conductivity measurements on template-free mesoporous ITO films were conducted following the Hall method (ECOPIA HMS 3000) using a magnetic field of 0.55 T.

Cyclic voltammograms were collected using a PARSTAT 2273 potentiostat with PowerSuite 2.56 software for data collection and analysis in a standard three-electrode electrochemical cell using Pt wire as

a counter electrode and Ag/AgCl/1M KCl as a reference electrode. Functionalized films on ITO glass used as working electrodes were masked with a Teflon-coated glass fiber tape leaving an exposed area of 0.75 cm^2.

References

1. H. Toraya, *J. Appl. Cryst.*, 1986, **19**, 440.
2. J. Laugier and B. Bochu, Laboratory of Materials and Physical Engineering, School of Physics, University of Grenoble, France, 2000.
3. G. K. Wertheim, M. A. Butler, K. W. Buchanan and D. N. E. West, *Rev. Sci. Instrum.*, 1974, **45**, 1369.
4. A. Le Bail, H. Duroy and J. L. Fourquet, *Mater. Res. Bull.*, 1988, **23**, 447.
5. A. C. V. D. Larson, R. B., in *Los Alamos National Laboratory Report*, 2001.
6. B. H. Toby, *J. Appl. Cryst.*, 2001, **34**, 210.
7. D. Balzar and H. Ledbetter, *J. Appl. Cryst.* , 1993, **26**, 97.
8. S. A. Howard, *Adv. X-Ray Anal.* , 1989, **32**, 523.
9. D. Balzar, *J. Appl. Cryst.* , 1992, **28**, 559.
10. D. Balzar, N. Audebrand, M. Daymond, A. Fitch, A. Hewat, J. I. Langford, A. Le Bail, D. Louër, O. Masson, C. N. McCowan, N. C. Popa, P. W. Stephens and B. H. Toby, *J. Appl. Cryst.* , 2004, **37**, 911.
11. P. Thompson, D. E. Cox and J. B. Hastings, *J. Appl. Cryst.* , 1987, **20**, 79.
12. B. E. Warren, *X-ray Diffraction. Reading*, MA. Addison-Wesley 1969.
13. D. L. Bish and J. E. Post, eds., *Modern powder diffraction, Reviews in Mineralogy*, Mineralogical society of America, Washington, 1989.
14. Y. Qiu, P. Bellina, L. P. H. Jeurgens, A. Leineweber, U. Welzel, P. Gerstel, L. Q. Jiang, P. A. van Aken, J. Bill, F. Aldinger, *Adv. Funct. Mater.* **2008,** *18*, 2572.
15. J. Rathouský, V. Kalousek, V. Yarovyi, M. Wark, J. Jirkovský, *J. Photochem. Photobiol. A.* **2010**, 216, 126.